JOURNAL OF SOLID STATE CHEMISTRY 42, 170–175 (1982)

Properties of β-Alumina Doped with Cerium

JOHN H. KENNEDY AND ANN M. SCHULER

Chemistry Department, University of California, Santa Barbara, California 93106

AND GEORGE E. CABANISS

Chemistry Department, University of North Carolina, Chapel Hill, North Carolina 27514

Received October 5, 1981

Cerium-doped β-alumina was prepared by sintering samples of β-alumina with Ce(III) nitrate or Ce(IV) oxide. The maximum solubility of cerium in β-alumina was determined to be ~10 w/o Ce using Vegard's Law. X-Ray absorption corrections were made for angles greater than 50°, using the wide-angle error function. The photoacoustic spectrum of cerium-doped β-alumina was determined and was consistent with the uv-visible absorption spectrum of Ce(IV) in an oxide lattice. Magnetic susceptibility measurements also indicated the existence of Ce(IV) in the β-alumina lattice. Conductivity values were measured on samples containing 2 and 4 w/o cerium. A decrease in conductivity compared to undoped β-alumina was similar to that found for Cr(IV)-doped β-alumina.

Introduction

Recently, considerable interest has been shown in β-alumina doped with various transition metals for increasing ionic and/or electronic conductivity (*1–5*). When a transition metal ion is introduced into the lattice of β-alumina, it may substitute for the Al^{3+} in the spinel block. Addition of ions of a differing valence state has been shown to increase or decrease the ionic conductivity, resulting from charge compensation which must be maintained within the crystal. Ions with oxidation states less than +3 may be charge compensated by an increase in sodium ions in the conduction plane. For those metals with oxidation states greater than +3, charge balance may be achieved by a decrease in sodium concentration in the conduction plane. Alternate charge balance mechanisms involving oxygen interstitials will also lead to expected conductivity changes.

Although there has been much work done involving the effects of transition metal-doped β-alumina on conductivity, it would also be of interest to determine the maximum solubility of the dopant in the β-alumina crystal lattice. Using Vegard's Law, it is possible by X-ray diffraction to observe changes in the lattice constants with an increase in dopant concentration. Many of the transition metals studied in the past had small ionic radii (i.e., Cr^{4+}, Co^{2+}, Fe^{3+}), so changes in the lattice constant with increased dopant concentration were difficult to detect. The present work involves doping β-alumina with cerium and the effect of this relatively large ion on the *c*-axis lattice constant and the conductivity.

Experimental

Pure Alcoa XB-2 superground β-alumina powder was doped by the addition of cerium nitrate, $Ce(NO_3)_3 \cdot 6H_2O$, or cerium dioxide, CeO_2, in an acetone slurry. The

0022-4596/82/050170-06$02.00/0

powders were thoroughly mixed using an α-alumina mortar and pestle. The acetone was allowed to evaporate, and the powder was then calcined in air at 1100°C for 24 hr to decompose the nitrates or oxides. Samples of 2 and 4 w/o were prepared from the nitrate; all others were prepared from the oxide.

Samples used in conductivity studies were prepared by pressing the calcined powder in a KBr pellet die followed by isostatic pressing at 25,000 psi. The pellets were then packed in 300-mesh β-alumina and sintered at 1570°C for 2.5 hr. The sintered samples were yellow-green in color with densities of approximately 3.1–3.2 g/cm³. After sintering, the samples were polished with 320-, 400-, and 500-μm-mesh silicon carbide paper. Further polishing was done using 9-, 6-, and 3-μm diamond laps. Gold blocking electrodes were sputtered onto the pellets using a Hummer sputtering apparatus.

X-Ray powder diffraction studies were performed with a Philips X-ray diffractometer using a Debye–Scherrer camera. All X-ray powder patterns were obtained using chromium radiation.

All lines were indexed for angles >50° and a corresponding *a*- and *c*-axis value was determined using the equation for hexagonal crystal symmetry with least-squares fitting:

$$\frac{1}{d^2} = \frac{4(h^2 + hk + k^2)}{3a^2} + \frac{l^2}{c^2}.$$

It was found that the *a* axis showed very little change and was taken to be 5.59 Å for succeeding calculations. Large differences, however, were observed in the *c* axis as dopant concentration increased.

Errors due to absorption effects were corrected using the wide-angle error function (WAEF) (*6*),

$$\text{WAEF} = \frac{1}{2}\left(\frac{\cos^2\theta}{\sin\theta} + \frac{\cos^2\theta}{\theta}\right).$$

The WAEF was calculated for each line where $\theta \geq 50$. It was then plotted vs the *c*-axis lattice constant and extrapolated to the ordinate giving the corrected value as shown in Fig. 1.

Magnetic susceptibility measurements were carried out using a Cahn Electrobalance at 298°K. The susceptibility standard used was ferrous ammonium sulfate, $Fe(NH_4)_2(SO_4)_2 \cdot 6H_2O$. Corrections were made for the diagmagnetism of pure β-alumina.

All photoacoustic spectra were acquired using a Princeton Applied Research Model 6001 photoacoustic spectrometer system which uses a 1-kw electronically pulsed xenon arc lamp in a F/4.2 reflector as its excitation source. System optics provide 8-nm resolution in the 200- to 800-nm spectral range when equipped with 2.0-mm exit and entrance slits. Detection of the photoacoustic signal is achieved by amplification of the microphone transducer. Real time source compensation is obtained by ratioing each analytical channel output to that of the pyroelectric detection system in parallel with the analytical channel.

The PAR 6001 system software has three storage channels available. A reference channel (R) is used to store a spectrum of a

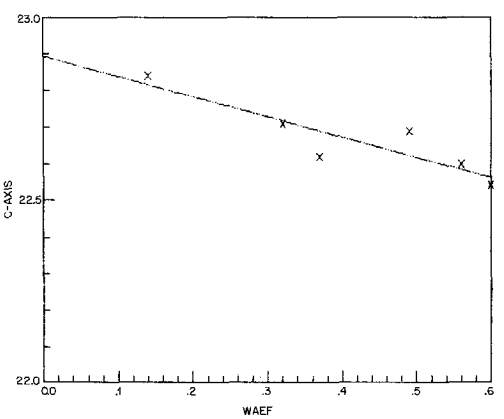

FIG. 1. Plot of *c* axis vs wide-angle error function for 12 w/o Ce-doped β-alumina.

black-body reference material (norite A, Fisher Scientific No. C-176). Signal-averaged spectra of undoped and doped β-alumina samples were acquired at 50-Hz (source) modulation frequency and stored in blank (B) and sample (S) channels, respectively. Signal ratio (S/R) or signal corrected for background ratio [(S-B)/R] were calculated internally from the stored data.

Conductivity measurements were made using a Solartron 1174 frequency response analyzer over the temperature range 25 to 300°C in a helium atmosphere. Complex impedance diagrams were interpreted using a computer program published previously (*7*).

A sodium analysis was carried out on all samples used in conductivity studies by an ion exchange method. Sintered pellets were immersed in molten $AgNO_3$ overnight, rinsed in distilled water and dilute HNO_3, and then reimmersed in fresh molten $AgNO_3$ for approximately 24 hr. The samples were then rinsed again and baked at 300°C overnight. Percentage Na^+ in each sample was then determined from the weight change that had occurred.

Results

X-Ray Diffraction

X-Ray powder patterns were taken on calcined samples over the range 2–20 w/o Ce. The *a*-axis lattice parameter remained essentially constant at 5.59 Å while values for the *c* axis increased linearly up to 10 w/o Ce following Vegard's Law. A decrease in the *c*-axis value was observed at $\geq$12 w/o Ce as shown in Fig. 2. All samples used in this study were checked by X-ray diffraction to determine if any α-alumina or β''-alumina was present, but none was found.

Magnetic Susceptibility

β-alumina samples doped with Ce(III) nitrate were used in magnetic susceptibility measurements. Powders that had been doped with Ce(III) and calcined at 1100°C for 24 hr were diamagnetic, showing no unpaired electrons. Powders containing Ce(III) that had not been calcined showed the presence of one unpaired electron.

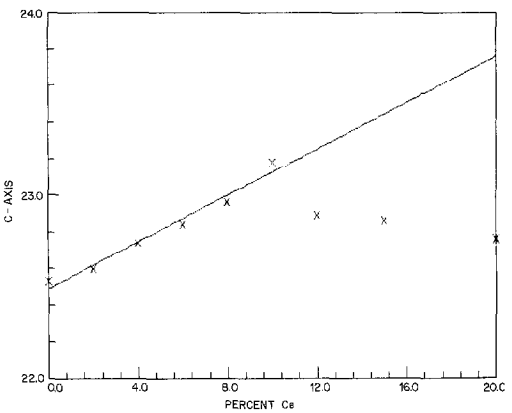

FIG. 2. Plot of c axis vs percentage Ce in β-alumina.

Photoacoustic Spectroscopy

A photoacoustic spectrum of 2 w/o Ce β-alumina from 350–700 nm is shown in Fig. 3. No absorption was observed >400 nm, while an intense absorption was noted at wavelengths below 400 nm. The absorption peak position could not be observed be-

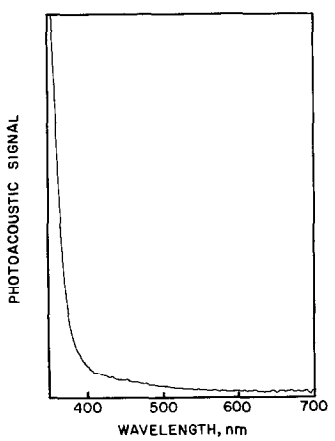

FIG. 3. Photoacoustic spectrum of 2 w/o Ce-doped β-alumina.

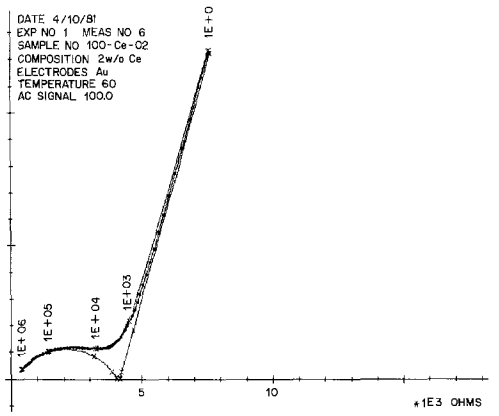

FIG. 4. Complex impedance diagram of 2 w/o Ce-doped β-alumina with sputtered gold electrodes at 60°C. Frequency range = 10^2–10^6 Hz. High-frequency intercept = 129 ohms (bulk resistance). Low-frequency intercept = 4.18×10^3 ohms (bulk plus grain-boundary resistance).

cause of the high absorptivity throughout the wavelength region accessible below 400 nm. Pure β-alumina, on the other hand, showed no absorption at wavelengths >325 nm.

Conductivity

A complex impedance plot for 2 w/o Ce β-alumina at 60°C is shown in Fig. 4. The bulk resistance was obtained by the extrapolation of the arc through the high-frequency points to the real axis. The low-frequency extrapolation gave the value of the bulk resistance plus that contributed by the grain boundaries.

Bulk and grain-boundary activation energies were determined from an Arrhenius plot of $\log \sigma T$ vs $1/T$ (°K). Conductivity and activation energies of Ce-doped β-alumina are compared to those of pure and Cr-doped β-alumina in Table I.

Sodium analysis of each sample used in conductivity measurements revealed that all pellets contained approximately 5.0 ± 0.1% Na.

Discussion

When β-alumina is doped with another high-oxidiation-state metal ion, the ion being introduced substitutes for the Al^{3+} in the spinel block. Doping β-alumina with Ce involves the substitution of an ion of radius 1.11 (Ce(III)) or 1.01 Å (Ce(IV)) for an Al^{3+} ion of radius 0.50 Å. By using Vegard's Law it was possible to detect expansion of the lattice constant as the concentration of Ce increased. The *c* axis increased linearly until the maximum solubility was reached. The little or no change in the *a*-axis lattice constant may probably be attributed to its low value, i.e., the measurements were not sufficiently sensitive to detect any change in the *a*-axis lattice constant. The large *c*-axis value, on the other hand, appears to be sensitive to substitution of dopant ions.

The solubility maximum occurred at approximately 10 w/o Ce. At 12 w/o a decrease was observed in the *c*-axis value and for higher concentrations little additional change was seen. The sharp decrease, fol-

TABLE I

CONDUCTIVITY DATA FOR Ce-DOPED β-ALUMINA COMPARED TO UNDOPED AND Cr-DOPED β-ALUMINA

Sample	σ_b (25°C) (sec-cm^{-1})	σ_b (300°C) (sec-cm^{-1})	σ_{gb} (25°C) (sec-cm^{-1})	E_a (bulk) (kcal/mole)	E_a (gb) (kcal/mole)
Pure β	1.1×10^{-3}	2×10^{-2}	7.3×10^{-4}	3.55	7.0
2 w/o Cr	0.9×10^{-3}	2×10^{-2}	6×10^{-4}	3.95	8.2
2 w/o Ce	1.2×10^{-3}	1.6×10^{-2}	3×10^{-4}	3.20	9.0
4 w/o Ce	0.83×10^{-3}	0.82×10^{-2}	0.02×10^{-4}	2.83	8.17

lowed by very little change in the lattice constant value, probably indicates the formation of a second phase, possibly of cerium oxide when the concentration exceeded 10 w/o. The lower value for the c axis observed at 12–20 w/o corresponds to about the value observed at 6 w/o Ce. This may indicate that with 6–10 w/o Ce the crystal is supersaturated and when precipitation of a second phase occurs at higher Ce concentrations, solid solution solubility drops to the 6 w/o value.

The oxidation state of Ce in the final sintered pellet was deduced from magnetic susceptibility and photoacoustic spectroscopy. The original powder containing Ce(III) was paramagnetic while the sintered material was diamagnetic, indicative of Ce(IV).

This oxidation number assignment was supported by the photoacoustic spectrum shown in Fig. 3. Cerium (III) in an oxide lattice (Y_2O_3) has been reported to give an absorption band between 350 and 500 nm caused by excitation of the f-level electron present (*8*). Weak absorption occurred at wavelengths <350 nm. On the other hand, 1 a/o Ce(IV) in this oxide lattice only shows an intense absorption beginning below 400 nm with a broad peak around 300 nm (*8*). Thus the spectrum shown in Fig. 3 is consistent with the presence of Ce(IV) in the β-alumina lattice.

As shown in Table I, conductivities of β-alumina doped with 2 w/o Ce as $Ce(NO_3)_3 \cdot 6H_2O$ closely parallel those of β-alumina doped with 2 w/o Cr(IV) (*9*). On the basis of the assignment that both Ce and Cr are oxidized to the +4 oxidation state during sintering, this similarity in conductivity is not surprising. Unlike metal ions with oxidation state +2, Ce and Cr do not produce an increase in bulk conductivity. In fact, higher concentrations of Ce showed a marked decrease in bulk conductivity. This would be expected if charge compensation for Ce(IV) was accomplished with a lower Na^+ concentration and/or an increase in oxygen interstitials. Since the concentration of Na^+ was lower than that of the undoped β-alumina (5.0 vs 5.5 w/o) the Na^+ compensation mechanism may be significant. However, little change in sodium content was observed with increasing cerium-doping level. Thus, charge compensation by additional oxygen interstitials cannot be ruled out and may play the dominant role at high Ce concentrations.

Grain-boundary conductivities for 2 w/o Cr- and Ce-doped β-alumina were close in value, whereas that of 4 w/o Ce had decreased by almost two orders of magnitude. It has previously been observed that increase in grain-boundary resistance occurs as dopant concentration is increased (*2*). This has been attributed to ionic blocking at the grain boundaries.

Activation energies for both bulk and grain-boundary conductivities for Ce-doped β-alumina are similar to those of Cr(IV). A decrease in the activation energy for both the bulk and the grain boundaries for the 4 w/o Ce-doped samples was observed which was also observed for the Cr(IV)-doped samples (*2*).

No electronic conductivity was detected in Ce-doped β-alumina from low-frequency admittance plots. That is, the conductance extrapolated to zero frequency was zero within experimental error.

In conclusion, substantial substitution of Ce(IV) for Al(III) in β-alumina was found possible up to a maximum of ~10 w/o. This would correspond to the formula $Na_{1.44}Ce_{0.47}Al_{10.53}O_{17.46}$ based on a sodium content of 5.0 w/o. As indicated by the formula, charge compensation appears to be primarily accomplished by oxide interstitials. However, the sodium content was also decreased somewhat from that of undoped β-alumina. Bulk conductivity was decreased by Ce substitution, and at high Ce-doping levels resistance at grain boundaries became extremely high.

Acknowledgments

The authors (J.H.K. and A.M.S.) acknowledge financial support of this project by the National Science Foundation, Grant DMR 80-02676. J.H.K. thanks the University of North Carolina, Chapel Hill, for a visiting professorship which promoted the joint work reported, and the authors thank Dr. R. A. Palmer and Dr. C. H. Lochmüller for the use of the photoacoustic spectroscopy equipment at Duke University.

References

1. W. L. Roth, W. C. Alexander, and S. J. LaPlace, Amer. Crystallogr. Assoc. Abstr. **2,** 1 (1973).
2. J. H. Kennedy, J. R. Akridge, and M. Kleitz, *Electrochim. Acta.* **24,** 781 (1979).
3. P. D. Dernier and J. P. Remeika, *J. Solid State Chem.* **17,** 245 (1976).
4. J. P. Boilot, A. Kahn, J. Thery, R. Collongues, J. Antoine, D. Vivien, C. Chevrette, and J. Gourier, *Electrochim. Acta.* **22,** 741 (1977).
5. J. R. Akridge, B. Srour, C. Meyer, Y. Gros, and J. H. Kennedy, *J. Solid State Chem.* **25,** 169 (1978).
6. H. P. Klug and L. E. Alexander, "X-Ray Diffraction Procedures," 2nd ed., pp. 594–595, Wiley, New York (1974).
7. M. Kleitz and J. H. Kennedy, "Fast Ion Transport in Solids" (P. Vashita, J. N. Mundy, and G. K. Shenoy, Eds.), pp. 185–188, Elsevier/North-Holland, Amsterdam (1979).
8. M. J. Fuller, *J. Electrochem. Soc.* **128,** 1381 (1981).
9. J. H. Kennedy and J. R. Akridge, *J. Solid State Chem.* **26,** 147 (1978).